Acta Biochim Biophys Sin 2023, 55(1): 154–161
https://doi.org/10.3724/abbs.2022156
Advance Access Publication Date: 2 November 2022
Short Communication

Short Communication

Nuclear localization of human MEIOB requires its NLS in the OB domain and interaction with SPATA22

Yating Xu[1,†], Zhen Chen[1,†], Panfeng Wu[1,†], Wei Qu[1,†], Hanqing Shi[1,†], Muyang Cheng[2], Yumin Xu[1], Tingyu Jin[1], Cong Liu[1], Cong Liu[1,*], Yi Li[3,*], and Mengcheng Luo[1,*]

[1]Hubei Provincial Key Laboratory of Developmentally Originated Disease, TaiKang Medical School (School of Basic Medical Sciences), Wuhan University, Wuhan 430071, China, [2]Zhongnan Hospital of Wuhan University, Wuhan 430071, China, and [3]Center for Reproductive Medicine, Sun Yat-sen Memorial Hospital, Sun Yat-sen University, Guangzhou 510120, China

[†]These authors contributed equally to this work.

*Correspondence address. Tel: +86-18507116557; E-mail: woshiziyoudeyulc@163.com (C.L.) / Tel: +86-16177126048; E-mail: liyi820920@126.com (Y.L.) / Tel: +86-18062582139; E-mail: luomengcheng@whu.edu.cn (M.L.)

Received 19 May 2022 Accepted 6 July 2022

Abstract

MEIOB is a vital protein in meiotic homologous recombination and plays an indispensable role in human gametogenesis. In mammals, MEIOB and its partner SPATA22 form a heterodimer, ensuring their effective localization on single-strand DNA (ssDNA) and proper synapsis processes. Mutations in human MEIOB (hMEIOB) cause human infertility attributed to the failure of its interaction with human SPATA22 (hSPATA22) and ssDNA binding. However, the detailed mechanism is still unclear. In our study, truncated or full-length hMEIOB and hSPATA22 are traced by fused expression with fluorescent proteins (i.e., copGFP or mCherry), and the live cell imaging system is used to observe the expression and localization of the proteins. When transfected alone, hMEIOB accumulates in the cytoplasm. Interestingly, a covered NLS in the OB domain of hMEIOB is identified, which can be exposed by hSPATA22 and is necessary for the nuclear localization of hMEIOB. When hSPATA22 loses its hMEIOB interacting domain or NLS, the nuclear localization of hMEIOB is aborted. Collectively, our results prove that the NLS in the OB domain of hMEIOB and interaction with hSPATA22 are required for hMEIOB nuclear localization.

Key words MEIOB, SPATA22, NLS, OB domain, protein interaction

Introduction

Meiosis is a specialized cell division process for human reproduction and is an essential part of generating haploid gametes [1–5]. During this process, meiotic recombination is critical for the fidelity of genetic information in the segregation of homologous chromosomes [2,6–8]. Therefore, the recombination process is precisely regulated and executed by numerous proteins, including double-strand break (DSB) repair-associated proteins [7–13]. Dysfunction of these proteins often results in a blocked response at different meiotic stages and ultimately leads to gametogenesis disorder. Therefore, studying the mechanism involved in DSB repair-associated proteins in gametogenesis is essential [14–16].

Meiosis-specific with OB domain-containing protein (MEIOB), which serves as an ssDNA-binding protein, is indispensable for DSB repair and meiotic recombination [17,18]. The completion of MEIOB function must rely on its partner, spermatogenesis-associated protein 22 (SPATA22) [19,20]. In most infertile cases caused by *MEIOB* or *SPATA22* mutation, the interaction between hMEIOB and hSPATA22 or the nuclear localization of hMEIOB is impaired [21–23]. Hence, it is generally accepted that the interaction between hMEIOB and hSPATA22 is a prerequisite for DSB repair [17,20,24]. However, the details, especially the nuclear localization mechanism, remain largely unknown.

To investigate the mechanism of the interaction and nuclear localization of hMEIOB and hSPATA22 during DSB repair, we used fluorescent proteins (i.e., CopGFP and mCherry) as labels to trace hMEIOB and hSPATA22 in living cells. Different segments of hMEIOB and hSPATA22 were used to characterize the sequence required for nuclear localization and reveal the underlying mechanism. Our study demonstrated the existence of a nuclear localization sequence (NLS) in the OB domain of hMEIOB that is necessary for the nuclear localization of hMEIOB. Interaction with

hSPATA22 may expose the NLS of hMEIOB and lead to nuclear localization of hMEIOB-hSPATA22.

Materials and Methods

Constructs

The DNA fragments coding the CopGFP and mCherry tags were amplified from the vectors pCDH-EF1-copGFP (plasmid #73030; Addgene, Watertown, USA) and pCDH-EF1a-eFFly mCherry (plasmid #104833; Addgene) and inserted into the *Xho*I/*Xba*I sites of pcDNA3.1(+) (plasmid #V790-20; Addgene), respectively, to generate pcDNA3.1-CopGFP-C or pcDNA3.1-mCherry-C. The cDNA fragments coding full-length human RPA2, MEIOB and SPATA22 were inserted into the *Nhe*I/*Xho*I sites of pcDNA3.1-CopGFP-C or pcDNA3.1-mCherry-C. The coding sequences of truncated human MEIOB and SPATA22 were amplified from vectors using primers listed in Supplementary Table S1 and inserted into the *Nhe*I/*Xho*I sites of pcDNA3.1-copGFP-C or pcDNA3.1-mCherry-C. The vectors with point mutations, e.g., M1, M2 and M3, were generated from pcDNA3.1-MEIOB-CopGFP-C by PCR amplification with mismatched oligonucleotides shown in Supplementary Table S2.

Transfection, laser micro-irradiation and live cell imaging

NT2 (CRL-1973™), HeLa (CCL-2) and U2OS (HTB96™) cells were purchased from American Type Culture Collection (ATCC, Manassas, USA). Cells were cultured in DMEM (HyClone, Logan, USA) supplemented with 10% fetal bovine serum (FBS) and 100 U/ml penicillin and streptomycin in a humidified 5% CO_2 atmosphere. All kinds of cells were transfected using Lipofectamine™ 3000 reagent (Invitrogen, Carlsbad, USA) with an attached protocol and kept culturing in 35-mm glass-bottom dishes (Invitrogen) for 24 h. To generate DNA damage in cells, a micropoint laser illumination and ablation system (Oxford Instruments, Oxford, UK) was adopted. Then, a high-energy UV laser (75%, 15 Hz/50 μJ, 365 nm to 656 nm) was generated from the system and focused on the nucleus through the given light path of the microscope to generate DNA damage. The kinetics of protein recruitment with DNA damage could be detected with a research-grade inverted fluorescence microscope (IX71; Olympus, Tokyo, Japan) and recorded with software (Oxford Instruments, Oxford, UK). All images were collected at room temperature without any fixation using the same parameters.

Statistical analysis

Fluorescence signal values presented the average signal intensity of the nucleus or cytoplasm. The relative fluorescence intensities in the nucleus were ratios of the average signal intensity in the nucleus and cytoplasm. Thirty pictures in the corresponding group were used for statistical analysis. All statistical analyses were performed by using GraphPad Prism (v. 7.04) and MATLAB (v. 7.0). The differences between groups were compared by Student's *t*-test. All experiments were repeated three times.

Results

hSPATA22 promotes nuclear localization of hMEIOB during DSB repair

To investigate the mechanism of hMEIOB and hSPATA22 in DSB repair, we used plasmids encoding fluorescently labelled hMEIOB and hSPATA22. After cotransfection into U2OS cells, laser irradiation (i.e., laser micropoint damage, LMPD) was used to induce DSBs. hMEIOB and hSPATA22 were colocalized in the nucleus and showed significant linear distribution at DSB sites (Figure 1A). To assess the colocalization of hMEIOB and hSPATA22, a particular region spanning the nucleus and DSB sites was selected and converted to gray levels for intensity analysis. The results showed that the distribution of hMEIOB and hSPAT22 was highly consistent, indicating that hMEIOB and hSPATA22 could effectively enter the nucleus and localize to DSB sites (Figure 1B). Interestingly, localization at DSB sites was not observed when hMEIOB was transfected alone. hRPA2, a DSB repair-associated protein, served as a positive control and could be located at DSB sites (Figure 1C). Moreover, the distribution pattern of hMEIOB was very different from that of hSPATA22 (Figure 1D,E). To rule out interference from cell types, we mono-expressed or coexpressed hMEIOB-CopGFP with hSPATA22-mCherry in NT2, HeLa and U2OS cell lines. The imaging and statistical results demonstrated that hMEIOB alone could not enter the nucleus, and nuclear localization appeared only in the presence of hSPATA22 (Figure 1F–H). These results indicated that hMEIOB could enter the nucleus only with the assistance of hSPATA22 during DSB repair.

Truncated hMEIOB can enter the nucleus without the assistance of hSPATA22

As a DSB repair-associated protein, hMEIOB should be able to enter the nucleus guided by a nuclear localization sequence (NLS). To investigate the position of the NLS of hMEIOB, we segmented hMEIOB into three parts [i.e., N-terminal (aa 1–166), OB domain (aa 167–272, the ssDNA binding domain), and C-terminal (aa 273–471, the hSPATA22 interacting domain)] according to the function of hMEIOB [17,24]. These three parts were abbreviated as N, OB and C, respectively. We assembled the three parts into three new fragments (i.e., NOB, OBC, and NC). Likewise, these truncated hMEIOB formats were also fused with CopGFP (Figure 2A). After transfection, the N, C and NC were mainly distributed in the cytoplasm. In contrast, the truncated isoforms with the OB domain were distributed in the nucleus and cytoplasm (Figure 2B–D). To further verify the DSB binding ability of NOB, OB and OBC, we used laser irradiation to generate DSBs and monitored the DSB localization of these truncated isoforms (Figure 2E). Compared with OB, the NOB and OBC isoforms showed an obvious DSB localization pattern. To explore the role of hSPATA22 in hMEIOB nuclear localization, we cotransfected hSPATA22-mCherry with NC and OBC (Figure 2F). Although the domain interacting with hSPATA22 was retained in NC and OBC, there was little change compared with the mono-transfection of NC and OBC (Figure 2G, H). These results suggested that truncated hMEIOB could enter the nucleus, which is guided by its OB domain that may contain the NLS.

hMEIOB has a covered NLS in the OB domain

To explore the molecular mechanism of the NLS in the OB domain in guiding the nuclear localization of hMEIOB, we analyzed the role of the distribution of basic amino acids (BAAs) in the OB domain (Figure 3A). In recent years, protein structure prediction has greatly aided protein functional studies. The new and efficient prediction tools, e.g., AlphaFold, can compute the possible structure with a high confidence score. To obtain information about the structural information of hMEIOB, we performed protein structure prediction online (https://alphafold.ebi.ac.uk/entry/Q8N635). The OB segment had high pLDDT (a per-residue confidence score) in the

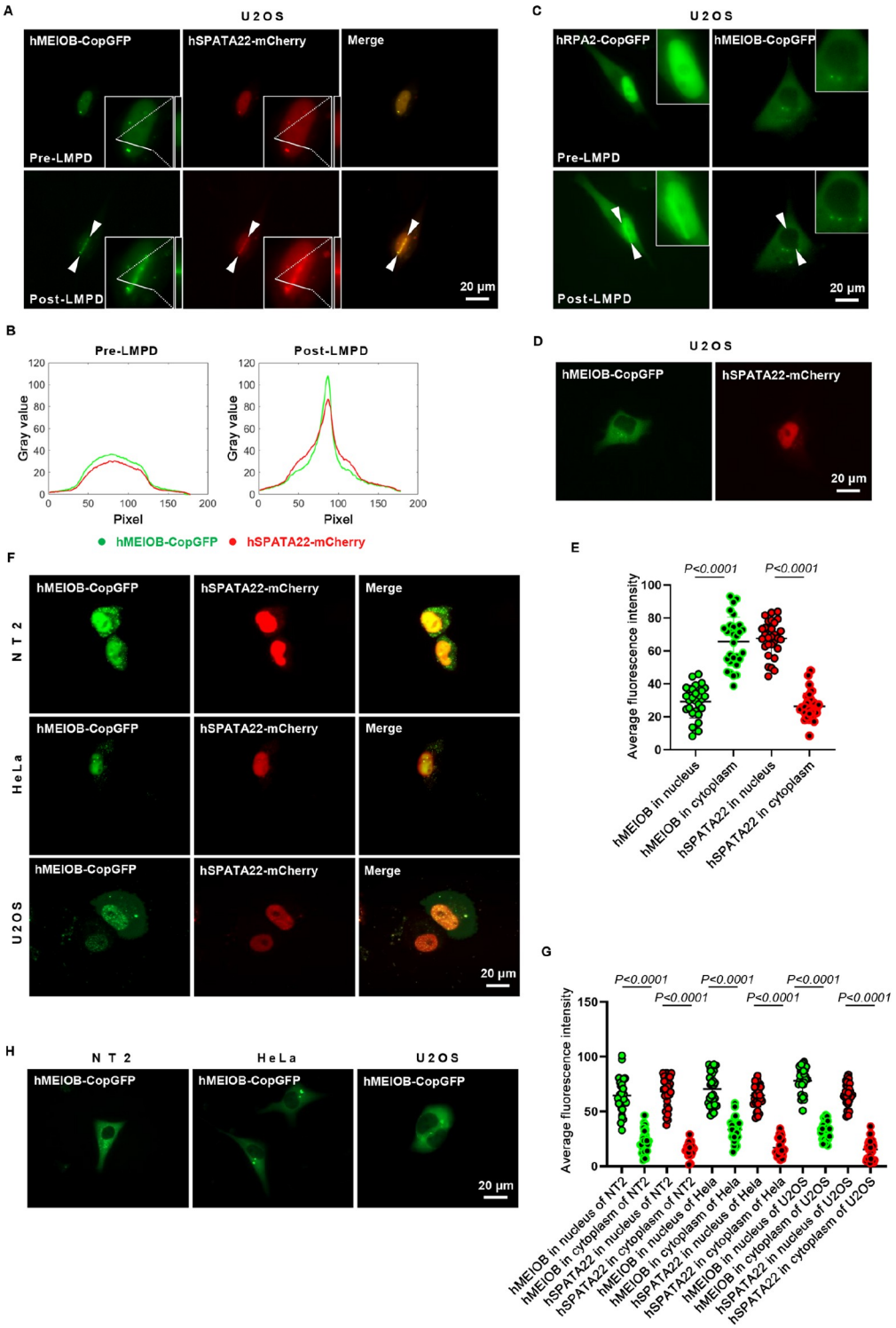

Figure 1. Different intracellular locations of hMEIOB after transfection with or without hSPATA22 (A) The coexpression of hMEIOB-CopGFP (green) and hSPATA22-mCherry (red) in U2OS cells and localization before and after LMPD. The zoomed regions are in the lower right corner. Double white triangles indicate the damage path. White lines and the zoomed areas are used for analyzing identity. (B) Fluorescence intensity analysis of hMEIOB and hSPATA22 before and after LMPD. The abscissa of each point corresponds to the path of the white line in A. The ordinate is the average gray value of intensity. (C) The distribution of hRPA2-CopGFP and hMEIOB-CopGFP before and after LMPD. The zoomed regions are in the upper right corner. (D) The distribution of hMEIOB-CopGFP or hSPATA22-mCherry in U2OS cells. (E) Statistics of the distribution of hMEIOB-CopGFP or hSPATA22-mCherry in the cytoplasm and nucleus individually expressed in U2OS cells. (F) The coexpression of hMEIOB-CopGFP and hSPATA22-mCherry in different cell lines, i.e., NT2, HeLa and U2OS cells. (G) Statistics of the distribution of hMEIOB-CopGFP and hSPATA22-mCherry in the cytoplasm and nucleus coexpressed in NT2, HeLa and U2OS cells. (H) The expression of hMEIOB-CopGFP alone in NT2, HeLa and U2OS cells. In E and G, the statistical results (mean ± SD) and differences (*P* values) between groups are shown ($n = 30$). Scale bar: 20 μm.

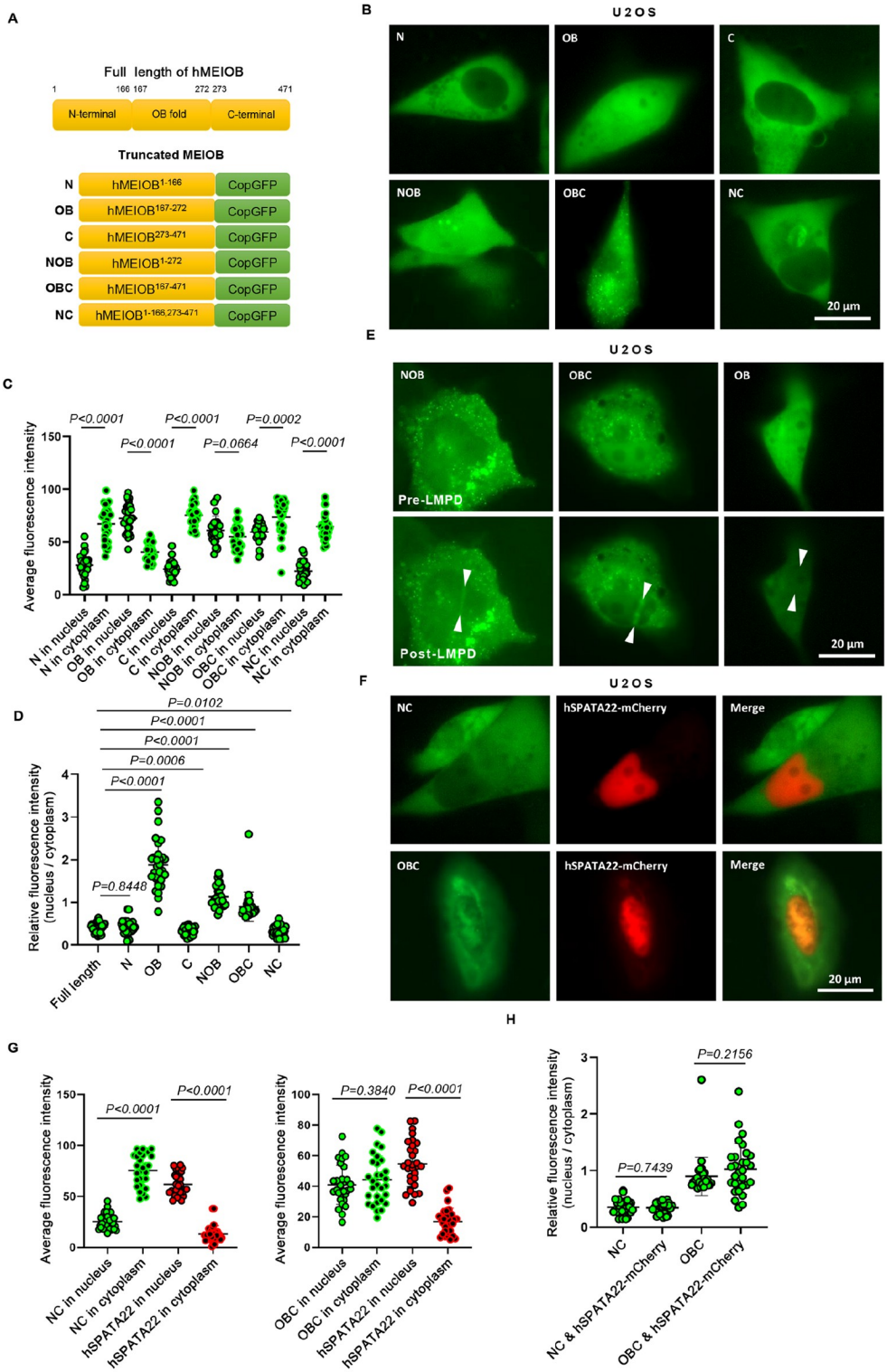

Figure 2. The truncated hMEIOB exhibited different localizations in cells without hSPATA22 (A) Full-length hMEIOB is segmented and used for constructing the CopGFP fused isoforms. (B) The distribution of various truncated hMEIOB-CopGFP (green) in U2OS cells. (C) Statistics of the distribution of various truncated hMEIOB in the cytoplasm and nucleus expressed in U2OS cells. (D) Statistics of the relative fluorescence intensity ($F_{nucleus}/F_{cytoplasm}$) of full-length and various truncated hMEIOB-CopGFP expressed in U2OS cells. (E) The distribution of OB, NOB and OBC in U2OS before and after LMPD. (F) The distribution of NC or OBC coexpressed with hSPATA22-mCherry in U2OS cells. (G) Statistics of the distribution of truncated hMEIOB (NC and OBC) and hSPATA22 in the cytoplasm and nucleus expressed in U2OS cells. (H) Statistics of the relative fluorescence intensity ($F_{nucleus}/F_{cytoplasm}$) of NC and OBC coexpressed with or without hSPATA22-mCherry. In C, D, G and H, the statistical results (mean ± SD) and differences (*P* values) between groups are shown ($n = 30$). Scale bar: 20 μm.

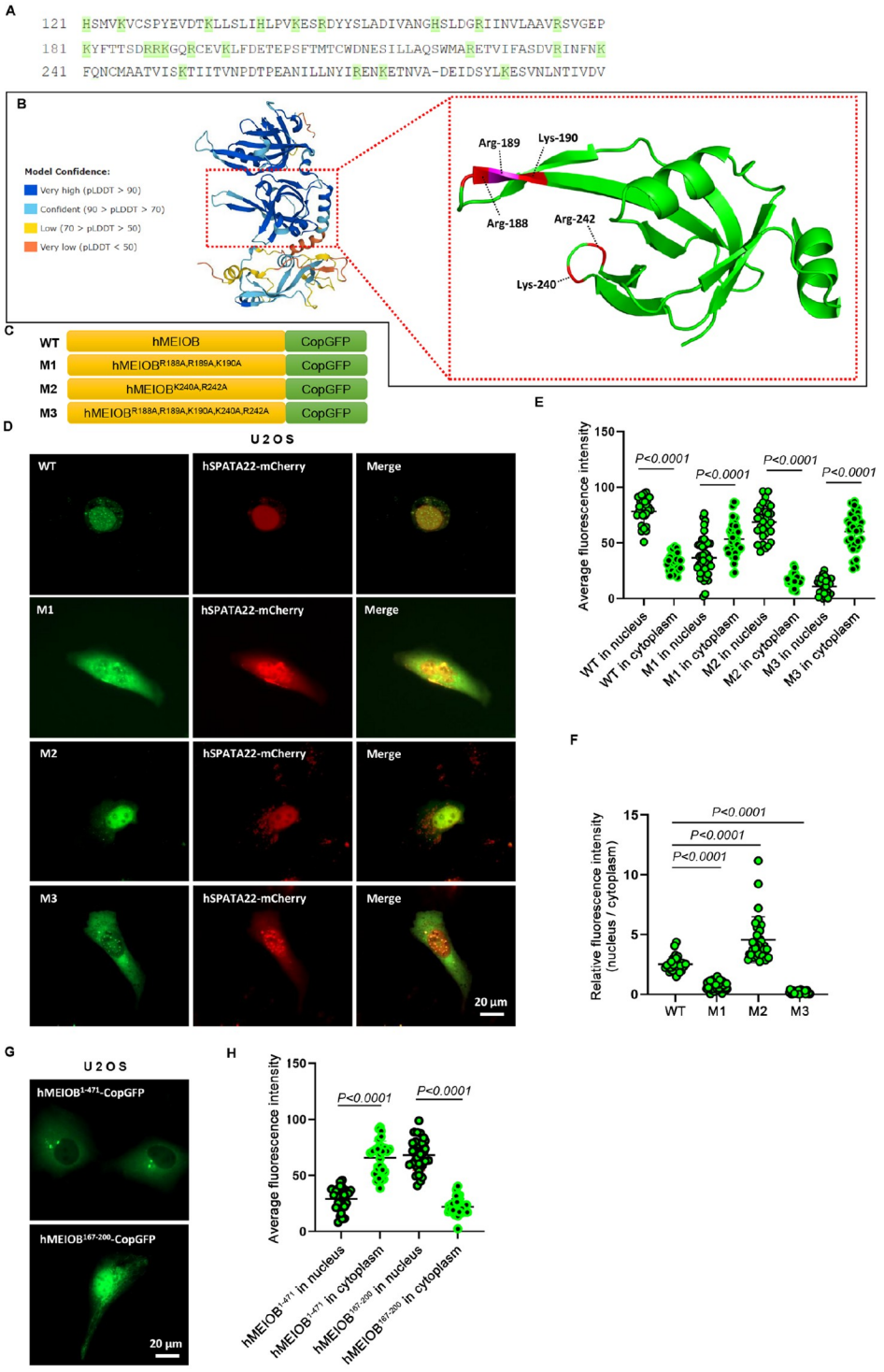

Figure 3. hMEIOB covered the nuclear localization sequence (NLS) in the OB domain (A) The distribution of basic amino acids among residues 121–260 of hMEIOB. The laurel-green label highlights the basic amino acids in the sequence. (B) The predicted structure of full-length hMEIOB by using AlphaFold. The chosen basic amino acids are labelled on the OB domain (right). (C) Normal and point-mutated full-length hMEIOB were fused with CopGFP. (D) The coexpression of hMEIOB-CopGFP (WT, M1, M2 or M3) and hSPATA22-mCherry in U2OS cells. (E) Statistics of the distribution of hMEIOB (WT, M1, M2 and M3) in the cytoplasm and nucleus coexpressed with hSPATA22 in U2OS cells. (F) Statistics of the relative fluorescence intensity ($F_{nucleus}/F_{cytoplasm}$) of hMEIOB-CopGFP (WT, M1, M2 and M3) coexpressed with hSPATA22-mCherry in U2OS cells. (G) Fluorescence distribution of hMEIOB (aa 167–200)-CopGFP and hMEIOB (aa 1–471)-CopGFP (control) in U2OS cells. (H) Statistics of the distribution of hMEIOB (aa 1–471)-CopGFP and hMEIOB (aa 167–200)-CopGFP in the cytoplasm and nucleus individually expressed in U2OS cells. In E, F and H, the statistical results (mean ± SD) and differences (*P* values) between groups are shown ($n = 30$). WT represents the normal hMEIOB-CopGFP, M1 represents the mutated hMEIOB^{R188A,R189A,K190A}-CopGFP, M2 represents the mutated hMEIOB^{K240A,R242A}-CopGFP and M3 represents the mutated hMEIOB^{R188A,R189A,K190A,K240A,R242A}-CopGFP. Scale bar: 20 μm.

prediction, of which the scores of most residues were above 90, and the rest were from 70 to 90 (Figure 3B). To investigate the underlying BAAs in the NLS, we aligned the accumulation areas of BAAs and positioned them on the structure and found two possible regions (Figure 3B). Then, we mutated the BAAs (188R, 189R, 190K, 240K, and 242R) to alanine (A) and coexpressed these mutated forms of full-length hMEIOB (M1, M2, and M3) with hSPATA22 (Figure 3C,D). The imaging results showed that the mutations of these BAAs led to a limitation in nuclear localization of hMEIOB, and mutations in M1 and M3 were more severe than those in M2 compared with WT (Figure 3E,F). To further verify the position of the NLS of hMEIOB, we expressed residues 167–200, which contain the BAAs mutated in M1 and fused with CopGFP for localization detection (Figure 3G). Imaging and statistical results indicated that this region (aa 167–200) could direct CopGFP to nuclear localization (Figure 3H). These data indicated that the NLS of hMEIOB is located in the OB domain, and mutations of NLS may not be remedied by hSPATA22.

The NLS and hMEIOB-interacting domain of hSPATA22 are necessary for the nuclear localization of the hMEIOB-hSPATA22 heterodimer

As shown in Figure 1, hSPATA22 promoted the nuclear localization of hMEIOB. To investigate the details of the assistance, we segmented hSPATA22 and found the NLS (aa 1–31) of hSPATA22 (Figure 4B). According to a previous study [24], we expressed the hMEIOB-interacting domain of hSPATA22 (aa 237–363). The above segments, full-length hSPATA22 and the other two remaining segments of hSPATA22 (aa 32–363 and aa 1–236), were fused with CopGFP, and full-length hMEIOB was fused with mCherry (Figure 4A,B). The nuclear localization of hMEIOB was limited when hSPATA22 lost its NLS- or hMEIOB-interacting domain (Figure 4C–E). Interestingly, the nuclear localization of hMEIOB was remarkable when coexpressed with hSPATA22 (aa 1–31 and aa 237–363). These results indicated that hSPATA22 could promote the nuclear localization of hMEIOB, which requires the NLS- and hMEIOB-interacting domains of hSPATA22.

Discussion

In the current study, we proved that full-length hMEIOB mainly accumulated in the cytoplasm without hSPATA22. When hMEIOB and hSPATA22 were coexpressed, this heterodimer could enter the nucleus and be enriched at DSB sites. Consistently, mutated hMEIOB, which lacks the hSPATA22-interacting domain, will abnormally accumulate in the cytoplasm [22]. These data suggested that hSPATA22 could assist hMEIOB in nuclear localization (Figure 5).

Proteins localized in the nuclear often have an NLS, which would lead to its nuclear localization. There are also exceptional cases in which some proteins have cryptic NLSs, which would be exposed to the surface of proteins through different mechanisms, such as dissociation of the inhibiting subunits [25]. Interestingly, the truncated hMEIOB (i.e., NOB, OBC, and OB) could achieve nuclear localization, which indicated that hMEIOB has a covered NLS in the OB domain. This result is consistent with the finding that other fragments (i.e., NC, N and C) could not localize to the nucleus. In addition, the low efficiency of nuclear localization of NOB and OBC may also imply that the exposure of NLS is inadequate. Moreover, NOB and OBC could also be enriched at DSB sites without the help of hSPATA22, which implies that the OB domain may need flanking sequences for a sufficient ssDNA binding ability [17]. It is well known that karyophilic residue clusters composed of arginines and lysines should be contained in the NLS [26]. The distribution of the clusters in the OB domain may present as a separated state, as bipartite NLSs were discovered in XRCC1 and Ku70, which also participate in the DSB repair process [27,28]. Because the loss of NLS limits the nuclear localization of proteins [29,30], the mutated full-length hMEIOB with mutations at the chosen arginines and lysines exhibited limited nuclear localization. Consistently, the fragment (aa 167–200) of hMEIOB containing the predicted NLS can effectively lead copGFP into the nucleus. Therefore, our data confirmed that hMEIOB has a covered NLS in the OB domain.

The interaction between proteins may change the protein conformation, which is essential for special functions [31,32]. Loss of the hMEIOB-interacting domain leads to disruption of the interaction between hMEIOB and hSPATA22, and hMEIOB is not distributed in the nucleus. Therefore, we speculate that hSPATA22 may expose the NLS of hMEIOB when interacting with it. Puzzlingly, the presence of the hMEIOB-interacting domain (aa 32–363 or aa 237–363 of hSPATA22) alone did not promote the nuclear localization of full-length hMEIOB. This led us to notice the importance of the NLS of hSPATA22. hMEIOB can enter the nucleus effectively only when the hSPATA22 fragment contains both the NLS (aa 1–31) and the hMEIOB-interacting domains (aa 237–363). However, it seems that hSPATA22 does not further improve the efficiency of the nuclear localization of truncated hMEIOB (i.e., OBC), which may indicate that the N segment of hMEIOB participates in its NLS exposure. Therefore, our data demonstrated that hSPATA22 assists hMEIOB nuclear localization and that the NLS- and hMEIOB-interacting domains are required during this process (Figure 5).

Supplementary Data

Supplementary data is available at *Acta Biochimica et Biophysica Sinica* online.

Acknowledgement

We would like to thank Dr. Wen-chang Zhang (Medical Research Institute, Wuhan University, Wuhan, China) for his technical assistance.

Funding

This work was supported by the grants from the National Natural Science Foundation of China (No. 31771588), the Strategic Collaborative Research Program of the Ferring Institute of Reproductive Medicine (No. FIRMC200509), the Key Research and Development Project of Hubei Province (No. 2021BCA111), and the Translational Medicine and Interdisciplinary Research (No. ZNJC201928) to M.L.

Conflict of Interest

The authors declare that they have no conflict of interest.

References

1. Ohkura H. Meiosis: An overview of key differences from mitosis. *Cold Spring Harb Perspect Biol* 2015, 7: a015859
2. Bolcun-Filas E, Handel MA. Meiosis: the chromosomal foundation of reproduction. *Biol Reprod* 2018, 99: 112–126
3. Clift D, Schuh M. Restarting life: Fertilization and the transition from

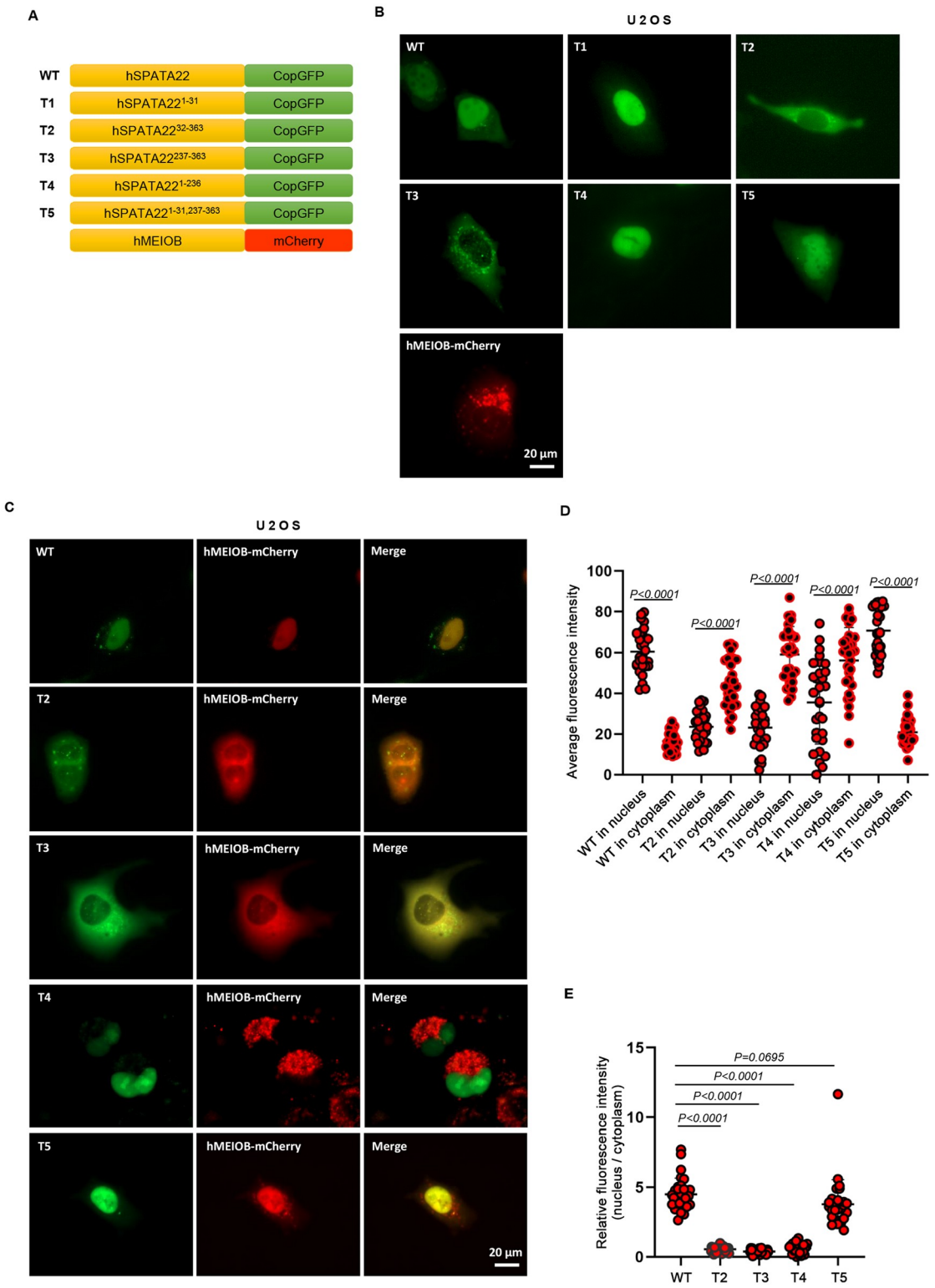

Figure 4. The NLS- and hMEIOB-interacting domains of hSPATA22 are required for hMEIOB to enter the nucleus (A) The diagram shows various truncated or full-length hSPATA22-CopGFP and full-length hMEIOB-mCherry. (B) Fluorescence distribution of various hSPATA22-CopGFP (green) and full-length hMEIOB-mCherry (red) in U2OS cells. (C) The coexpression of various hSPATA22-CopGFP and full-length hMEIOB-mCherry in U2OS cells. (D) Statistics of the distribution of hMEIOB-mCherry in the cytoplasm and nucleus in U2OS cells coexpressed with various hSPATA22-CopGFP. (E) Statistics of the relative fluorescence intensity ($F_{nucleus}/F_{cytoplasm}$) of hMEIOB-mCherry coexpressed with various hSPATA22-CopGFP. In D and E, the statistical results (mean ± SD) and differences (*P* values) between groups are shown ($n = 30$). WT represents the normal hSPATA22-CopGFP, T2 represents the truncated hSPATA22$^{32–363}$-CopGFP, T3 represents the truncated hSPATA22$^{237–363}$-CopGFP, T4 represents the truncated hSPATA22$^{1–236}$-CopGFP, T5 represents the truncated hSPATA22$^{1–31,237–363}$-CopGFP. Scale bar: 20 μm.

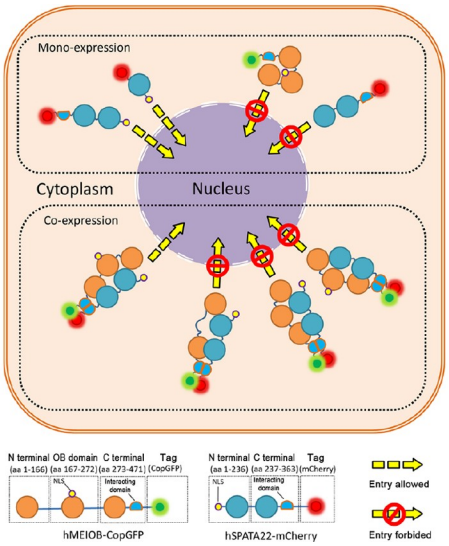

Figure 5. Schematic diagram of the entry of HMEIOB and hSPATA22 into the nucleus

meiosis to mitosis. *Nat Rev Mol Cell Biol* 2013, 14: 549–562

4. Le Bouffant R, Guerquin MJ, Duquenne C, Frydman N, Coffigny H, Rouiller-Fabre V, Frydman R, ***et al.*** Meiosis initiation in the human ovary requires intrinsic retinoic acid synthesis. *Hum Reprod* 2010, 25: 2579–2590
5. de Kretser DM, Loveland KL, Meinhardt A, Simorangkir D, Wreford N. Spermatogenesis. *Hum Reprod* 1998, 13 Suppl 1: 1–8
6. Zickler D, Kleckner N. Recombination, pairing, and synapsis of homologs during meiosis. *Cold Spring Harb Perspect Biol* 2015, 7: a016626
7. Hunter N. Meiotic recombination: the essence of heredity. *Cold Spring Harb Perspect Biol* 2015, 7: a016618
8. Handel MA, Schimenti JC. Genetics of mammalian meiosis: regulation, dynamics and impact on fertility. *Nat Rev Genet* 2010, 11: 124–136
9. Mishra G, Bigman LS, Levy Y. SsDNA diffuses along replication protein A via a reptation mechanism. *Nucleic Acids Res* 2020, 48: 1701–1714
10. Bonilla B, Hengel SR, Grundy MKK, Bernstein KA. *RAD51* gene family structure and function. *Annu Rev Genet* 2020, 54: 25–46
11. Hinch AG, Becker PW, Li T, Moralli D, Zhang G, Bycroft C, Green C, ***et al.*** The configuration of RPA, RAD51, and DMC1 binding in meiosis reveals the nature of critical recombination intermediates. *Mol Cell* 2020, 79: 689–701.e10
12. Chen H, He C, Wang C, Wang X, Ruan F, Yan J, Yin P, ***et al.*** RAD51 supports DMC1 by inhibiting the SMC5/6 complex during meiosis. *Plant Cell* 2021, 33: 2869–2882
13. Zhao W, Steinfeld JB, Liang F, Chen X, Maranon DG, Jian Ma C, Kwon Y, ***et al.*** BRCA1–BARD1 promotes RAD51-mediated homologous DNA pairing. *Nature* 2017, 550: 360–365
14. Ibtisham F, Honaramooz A. Spermatogonial stem cells for *in vitro* spermatogenesis and *in vivo* restoration of fertility. *Cells* 2020, 9: 745
15. Shiraishi K, Matsuyama H. Gonadotoropin actions on spermatogenesis and hormonal therapies for spermatogenic disorders. *Endocr J* 2017, 64: 123–131
16. Li L, Yang R, Yin C, Kee K. Studying human reproductive biology through single-cell analysis and in vitro differentiation of stem cells into germ cell-like cells. *Hum Reprod Update* 2020, 26: 670–688
17. Luo M, Yang F, Leu NA, Landaiche J, Handel MA, Benavente R, La Salle S, ***et al.*** MEIOB exhibits single-stranded DNA-binding and exonuclease activities and is essential for meiotic recombination. *Nat Commun* 2013, 4: 2788
18. Souquet B, Abby E, Hervé R, Finsterbusch F, Tourpin S, Le Bouffant R, Duquenne C, ***et al.*** MEIOB targets single-strand DNA and is necessary for meiotic recombination. *PLoS Genet* 2013, 9: e1003784
19. La Salle S, Palmer K, O'Brien M, Schimenti JC, Eppig J, Handel MA. Spata22, a novel vertebrate-specific gene, is required for meiotic progress in mouse germ cells1. *Biol Reprod* 2012, 86: 45
20. Xu Y, Greenberg RA, Schonbrunn E, Wang PJ. Meiosis-specific proteins MEIOB and SPATA22 cooperatively associate with the single-stranded DNA-binding replication protein A complex and DNA double-strand breaks†. *Biol Reprod* 2017, 96: 1096–1104
21. Wu Y, Li Y, Murtaza G, Zhou J, Jiao Y, Gong C, Hu C, ***et al.*** Whole-exome sequencing of consanguineous families with infertile men and women identifies homologous mutations in *SPATA22* and *MEIOB*. *Hum Reprod* 2021, 36: 2793–2804
22. Caburet S, Todeschini AL, Petrillo C, Martini E, Farran ND, Legois B, Livera G, ***et al.*** A truncating MEIOB mutation responsible for familial primary ovarian insufficiency abolishes its interaction with its partner SPATA22 and their recruitment to DNA double-strand breaks. *EBioMedicine* 2019, 42: 524–531
23. Gershoni M, Hauser R, Barda S, Lehavi O, Arama E, Pietrokovski S, Kleiman SE. A new *MEIOB* mutation is a recurrent cause for azoospermia and testicular meiotic arrest. *Hum Reprod* 2019, 34: 666–671
24. Ribeiro J, Dupaigne P, Petrillo C, Ducrot C, Duquenne C, Veaute X, Saintomé C, ***et al.*** The meiosis-specific MEIOB–SPATA22 complex cooperates with RPA to form a compacted mixed MEIOB/SPATA22/RPA/ssDNA complex. *DNA Repair* 2021, 102: 103097
25. Boulikas T. Nuclear localization signals (NLS). *Crit Rev Eukaryot Gene Expr*, 1993, 3: 193
26. Boulikas T. Putative nuclear localization signals (NLS) in protein transcription factors. *J Cell Biochem* 1994, 55: 32–58
27. Kirby TW, Gassman NR, Smith CE, Pedersen LC, Gabel SA, Sobhany M, Wilson SH, ***et al.*** Nuclear localization of the DNA repair scaffold XRCC1: uncovering the functional role of a bipartite NLS. *Sci Rep* 2015, 5: 13405
28. Koike M, Ikuta T, Miyasaka T, Shiomi T. The nuclear localization signal of the human Ku70 is a variant bipartite type recognized by the two components of nuclear pore-targeting complex. *Exp Cell Res* 1999, 250: 401–413
29. Vancurova I, Jochova J, Lou W, Paine PL. An NLS is sufficient to engage facilitated translocation by the nuclear pore complex and subsequent intranuclear binding. *Biochem Biophys Res Commun* 1994, 205: 529–536
30. Subramaniam PS, Larkin J, Mujtaba MG, Walter MR, Johnson HM. The COOH-terminal nuclear localization sequence of interferon gamma regulates STAT1 alpha nuclear translocation at an intracellular site. *J Cell Sci* 2000, 113: 2771–2781
31. Li F, Higgs HN. The mouse Formin mDia1 is a potent actin nucleation factor regulated by autoinhibition. *Curr Biol* 2003, 13: 1335–1340
32. Otomo T, Tomchick DR, Otomo C, Machius M, Rosen MK. Crystal structure of the Formin mDia1 in autoinhibited conformation. *PLoS ONE* 2010, 5: e12896